Is the Protein Surrounding the Active Site Critical for Hydrogen Peroxide Reduction by Selenoprotein Glutathione Peroxidase? An ONIOM Study

Rajeev Prabhakar,[†] Thom Vreven,[‡] Michael J. Frisch,[‡] Keiji Morokuma,[†] and Djamaladdin G. Musaev*,[†]

Cherry Emerson Center for Scientific Computation and Department of Chemistry, Emory University, Atlanta, Georgia 30322, and Gaussian, Inc., 340 Quinnipiac Street, Building 40, Wallingford, Connecticut 06492

Received: March 28, 2006; In Final Form: May 12, 2006

In this ONIOM(QM:MM) study, we evaluate the role of the protein surroundings in the mechanism of H_2O_2 reduction catalyzed by the glutathione peroxidase enzyme, using the whole monomer (3113 atoms in 196 amino acid residues) as a model. A new optimization scheme that allows the full optimization of transition states for large systems has been utilized. It was found that in the presence of the surrounding protein the optimized active site structure bears a closer resemblance to the one in the X-ray structure than that without the surrounding protein. H_2O_2 reduction occurs through a two-step mechanism. In the first step, the selenolate anion ($E-Se^-$) formation occurs with a barrier of 16.4 kcal/mol and is endothermic by 12.0 kcal/mol. The Gln83 residue plays the key role of the proton abstractor, which is in line with the experimental suggestion. In the second step, the O−O bond is cleaved, and selenenic acid (R−Se−OH) and a water molecule are formed. The calculated barrier for this process is 6.0 kcal/mol, and it is exothermic by 80.9 kcal/mol. The overall barrier of 18.0 kcal/mol for H_2O_2 reduction is in reasonable agreement with the experimentally measured barrier of 14.9 kcal/mol. The protein surroundings has been calculated to exert a net effect of only 0.70 kcal/mol (in comparison to the "active site only" model including solvent effects) on the overall barrier, which is most likely due to the active site being located at the enzyme surface.

I. Introduction

The understanding of the catalytic functioning of enzymes is a prime objective in biomolecular science. In the past decade, significant developments have transformed computational quantum chemistry into a powerful tool in the study of catalytic mechanisms of enzymatic reactions. The following two theoretical approaches have been widely employed in the investigation of enzyme-catalyzed reactions: (1) the "active site only" QM approach and (2) the hybrid quantum mechanics/molecular mechanics (QM/MM) approach. In the active site only QM approach, the enzyme active site is modeled using from tens to a hundred atoms and treated with high-level ab initio, density functional theory, or semiempirical methods. The active site only QM approach can be applied in two versions: (a) All structures (reactants, transition states, intermediates, and products) are fully optimized in a vacuum. In this approach, both the steric and electronic effects of the protein environment beyond the model are completely neglected. (b) The positions of some atoms, connected to backbones of active site amino acid residues, are frozen based on available X-ray structures, which preserves to some extent the steric effects of the protein environment.[1] In both the "fully optimized" and "partially frozen" approaches, the neglected electronic effects can be approximately incorporated using continuum dielectric medium methods.[2] Over the years these techniques have been used in the elucidation of a wide variety of biochemical processes.[3−9] However, the actual effect of the environment on the energetic and reaction mechanism is not always small, and often it is highly desired to model these effects explicitly.

Hybrid QM/MM methods can be used to improve the active site only models in the study of enzymatic reactions.[10−14] This approach allows the explicit inclusion of both steric and electrostatic effects from the protein surroundings. The entire system (referred to as the "real system") is divided into two subsystems. First, the QM region (or model system) contains the active site and is treated by quantum mechanics. Second, the MM region is treated with an empirical force field and contains the rest of the protein and eventually the solvent or other medium.

In this work we used the two-layer ONIOM(QM:MM) method.[15,16] The interface between the QM region and the MM region is treated by link atoms, and the interaction between the two layers is included at the classical level (mechanical embedding).[17] However, studying the full system in the same (static) way as an active site only model introduces a variety of challenges.[18] First, the conformational space of the protein environment is very extensive. Care must be taken that the energies that are compared correspond to the same configurations in the protein environment to ensure that energy differences between critical points on the potential surface reflect changes that are directly related to the reaction mechanism and not to arbitrary conformational changes. Second, the determination of energy barriers, which is essential for the understanding of reaction mechanisms, is very complicated for large systems. For small systems, such as the active site only models, there are standard tools available to locate transition states (TSs). These methods, however, have bottlenecks that do not allow them to

* Author to whom correspondence should be addressed. Phone: (404) 727-2382. E-mail: dmusaev@emory.edu.
[†] Emory University.
[‡] Gaussian, Inc.

10.1021/jp0619181 CCC: $33.50
Published on Web 06/16/2006

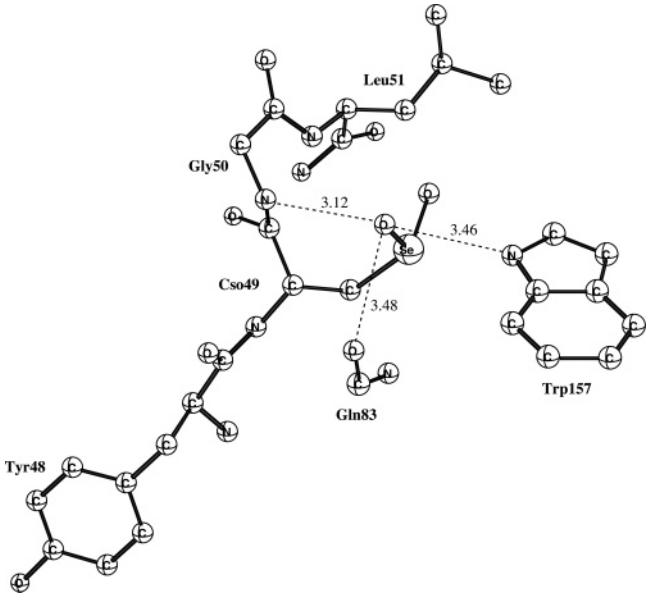

Figure 1. X-ray structure of the active site region of GPx.

be applied to systems containing thousands of atoms. As discussed below, we recently developed methods that remove the bottlenecks associated with the standard TS optimization scheme without compromising the accuracy. Our new methods allow the determination of true transition states on the QM/MM potential surface.

To evaluate the quantitative effect of the protein surroundings on the energetics of an enzymatic reaction, the catalytic mechanism of hydrogen peroxide reduction by glutathione peroxidase (GPx) has been investigated using the two-layer ONIOM(QM:MM) method. The ONIOM results are compared with both experiments and our previous findings using the active site only QM approach.

Glutathione peroxidase is a selenoprotein that protects cell membranes and other cellular components against oxidative damage.[19,20] The X-ray structures of bovine erythrocyte (intracellular enzyme) and human plasma (extracellular enzyme) GPx have been determined at 2.0 and 2.9 Å resolution, respectively.[21,22] However, of these two structures only the lower resolution (human plasma, 2.9 Å) GPx was solved for all the amino acid residues, and to facilitate modeling studies we recently refined its active site in an ONIOM study.[23] The occurrence of the selenocysteine residue is one of the peculiar features of the enzyme active site (Figure 1). Biochemical,[20] kinetic,[24] and crystallographic[21] studies on the bovine cellular enzyme indicate that this residue directly participates in the catalytic process of the reduction of hydroperoxide by GPx.

According to experiments, the catalytically active form of the enzyme is either the selenolate anion ($E-Se^-$) or selenol ($E-SeH$).[21] Hydroperoxide reduction by GPx can be formally described by the following reaction

$$E-Se-H + HOOH \rightarrow E-Se-OH + HOH \qquad (1)$$

In this reaction, the selenolate anion or selenol is oxidized to the selenenic acid with the concomitant reduction of hydrogen peroxide. The experimentally measured rate for H_2O_2 reduction of 0.51 s^{-1} corresponds to a barrier of 14.9 kcal/mol.[25]

Recently we investigated the entire catalytic cycle of GPx employing the active site only QM approach.[26] We predicted that the H_2O_2 reduction occurs through a stepwise mechanism in which the Gln83 residue acts as the proton acceptor, with an overall barrier of 17.1 kcal/mol. These results are in line with the available experimental data.[21] However, the effect of the protein environment on the energies and geometries of the proposed intermediates and transition states remains unclear. In the current paper we continue our computational investigation of the catalytic mechanism of this enzyme by including the complete protein environment in the calculations. The comparison of the ONIOM potential energy surface of reaction 1 with that reported in our previous study will allow us to assess the effect of the protein environment on the proposed mechanism.

II. Methods

A. The Coupled "Macro/microiterative" Geometry Optimization Scheme. In this section we describe the newly developed geometry optimization methods that were employed to obtain the minima and transition states reported in this work. Although standard methods are available for the optimization of minima on QM/MM potentials of large systems, they are usually not successful in locating transition states. We recently developed a scheme that is better suited for the optimization of those transition states.[27] We will first discuss standard TS and QM/MM geometry optimization schemes. This is followed by a brief discussion of the improvements introduced by our new scheme, which is discussed in detail in refs 27 and 28.

In standard TS geometry optimization methods,[29] the program first identifies the reaction coordinate (RC) vector, which corresponds to the normal mode with negative curvature. This mode is obtained by diagonalizing the Hessian matrix, the second derivative matrix of the energy with respect to the nuclear coordinates. The Hessian may be evaluated analytically, but it is usually obtained through an update mechanism using the gradients along the optimization path. The energy is then maximized in the direction of the RC vector and minimized in all other directions. This is an iterative process, and the RC vector needs to be reevaluated in each cycle. Because such an optimization scheme is second-order (it employs first and second derivatives, the gradients and Hessian) the computational time needed to compute the RC vector and the geometry step size scales at least cubically with the size of the system. This becomes a bottleneck for large systems, and this standard scheme can therefore not be applied to geometry optimization of structures such as those presented in this paper.

Second-order schemes are essential for TS searches, but they are also preferred for the optimization of minima. The inclusion of the second-order terms improves the convergence behavior significantly, and much fewer optimization cycles are required than in schemes using only first-order terms for the geometry step. Note that even an optimization scheme in which an updated Hessian is used and only the gradients are evaluated analytically is still second-order in the geometry step.

As stated before, standard second-order optimization schemes cannot be used for the large systems often studied with QM/MM methods. However, it turns out that QM/MM potentials can be efficiently optimized with a hybrid scheme that treats the QM region and the MM region with different types of optimizers. This scheme is known as "macro/microiteration".[15,30] First, a second-order geometry step (the macroiteration) is calculated for only the atoms in the QM region. Then, keeping the QM atoms fixed, the atoms in the MM region are fully minimized iteratively using a first-order method, the microiterations. These two steps are repeated until the forces on all the atoms are zero. It is clear that the efficiency of this scheme is the result of the difference in computational cost of the QM calculation and the MM calculation. Although many more MM

(inexpensive) calculations are needed, the overall computational time is reduced because the number of (expensive) QM steps is kept to a minimum.

Since in the hybrid macro/microiteration scheme a second-order method is used for the QM region, one could, in principle, carry out a TS optimization. However, a TS search using this approach has two major problems. First, since the Hessian only exists for the QM atoms, the RC vector is forced to be localized in the QM region. Although this may be a valid approximation in many cases, in some cases the true RC vector may extend over MM atoms as well. Second, TS searches depend critically on the quality of the Hessian, which is usually poor in the macro/microiteration scheme. The reason is that in the Hessian update mechanism the QM/MM forces (not the QM forces only) need to be used. These forces depend on both the QM and the MM coordinates, but the latter, however, are not included as variables in the Hessian update mechanism. This makes the updated Hessian ill-defined, resulting in poor convergence behavior. To conclude, it is generally not easy to locate TSs using the standard QM/MM macro/microiteration scheme. Below, we briefly describe our new and more rigorous scheme for QM/MM geometry optimization, which is also able to optimize TSs.

In our new approach, which may be called the "coupled macro/microiteration" scheme, we modify the macroiteration of the macro/microiteration scheme by explicitly including the coupling of the QM region with the MM region. In other words, we calculate the RC vector and macrostep using the full QM/MM Hessian and not just the Hessian for the QM part. Of course, here we would encounter again the cubic scaling problem as mentioned above, but we developed direct and linear scaling methods for the MM contributions to make this step feasible. The MM blocks in the Hessian are described using analytical second derivatives of the MM potentials. The inclusion of this coupling improves the convergence behavior and allows the RC vector to extend into the MM space. The Hessian matrix of the QM contribution can be either analytical or obtained by an update mechanism. We also changed this update mechanism, which is now well defined because it only uses the forces from the QM contribution to the QM/MM potential. In this scheme, the microiterations are retained but carried out orthogonal to the RC vector. The combination of an accurate Hessian, explicit coupling, and lifting the requirement that the RC vector is localized in the QM region resulted in a general and reliable scheme for the geometry optimization of transition states in QM/MM systems. Besides the optimization of transition states, the scheme also improves the minimization on QM/MM potential surfaces. This new optimization method can currently only be applied with a mechanical embedding (ME) scheme.

B. Computational Models. In the present study, the entire monomer of GPx, containing 3113 atoms in 196 amino acid residues, has been chosen as the "real" system and is extracted from the dimeric X-ray structure.[22] The choice of monomeric unit is justified by the fact that in the crystal structure of the mammalian GPx (2.9Å) the active site selenocysteine residues are well separated with a Se−Se distance of 23.2 Å. In the starting structure containing 196 amino acid residues, hydrogen atoms not included in the PDB structure were added using the GaussView program.[31]

The "active" QM part of the real system for ONIOM calculations is constructed by utilizing all the available experimental information. Since the selenocysteine residue is experimentally suggested to play a critical role in the catalytic cycle,[21,22] it is included in the active part. The active site Gln83 and Trp157 residues were experimentally suggested to be involved in the catalytic mechanism,[32] and their side chains are included in the active part. Apart from them, in the X-ray structure,[22] Tyr48, Gly50, and, Leu51 residues are shown to form a part of the cage around the selenocysteine residue; therefore they are also included in the active part. In the X-ray structure, the active site is located at the surface of the enzyme and is oriented in such a way that the Cso49-containing cage isolates the active site water molecules from rest of the monomer. As a result, an active site water molecule, previously proposed to participate in the mechanism,[26] is positioned in such a way that it can interact only with the Cso49-containing cage and not with the remaining part of the monomer (lying on the opposite side of the cage). Therefore, the water molecule is not included in the models used in the proposed calculations. However, it is a reasonable to include the effect of the water molecule on all the present ONIOM structures from the active site only calculations that include the water molecule. The constructed system consists of 3113 atoms including 86 atoms in the active QM region and the rest in the MM region. The overall charge of the system as well as the active part used in the calculations is neutral.

C. Computational Procedures. All the calculations were performed using a development version of the Gaussian03 program package.[33] The active part is treated at the B3LYP level[34] using the 6-31G(d) basis set. The real system is treated at the MM level using the Amber force field. Standard Amber parameters have been used, except for the atoms present in the active site selenocysteine residue (see ref 35 for details).

All degrees of freedom were optimized, and for each TS we confirmed that the imaginary frequency corresponds to the reaction coordinate. The final energetics of the optimized structures were improved by including single-point energies using the triple-ζ 6-311+G(d,p) basis set, unscaled zero-point energy, and thermal corrections (at 298.15 K and 1 atm) estimated at the B3LYP/6-31G(d) level from the active site only study.[26]

We need to consider certain aspects related to the methods that we used. First, the conformational space of the protein environment is large, and we must ensure that relative energies refer to the same local minimum. Second, the MM atom types of some active site atoms formally change during the reaction. Despite these centers being part of the QM region, they can to some extent affect the energetics of the reaction.[36,37] As a measure for the reaction proceeding in the same conformation space, we calculated the root-mean-square (RMS) deviation of the MM part (including hydrogen atoms) of every single structure and compared it with the previous one. The effects of changes in MM parameters are included in the reported energies, and the specific contributions are estimated by calculating the barriers with the two alternative sets of parameters. In addition the effect of the aforementioned water molecule on the energetics is included from the active site only study. Throughout the paper, energies including all the above-mentioned effects are used, while the energies without the inclusion of surrounding protein (from the active site only calculations) are provided in parentheses.

We have previously demonstrated the applicability of the ONIOM (B3LYP:Amber) method in describing the structure of an enzyme for bacteriorhodopsin,[38] methane monooxygenase,[39] ribonucleotide reductase,[39] mammalian GPx,[23] *E. coli* NifS CsdB protein,[1] methylmalonyl-CoA mutase,[40] and lysine carboxylation in proteins.[41]

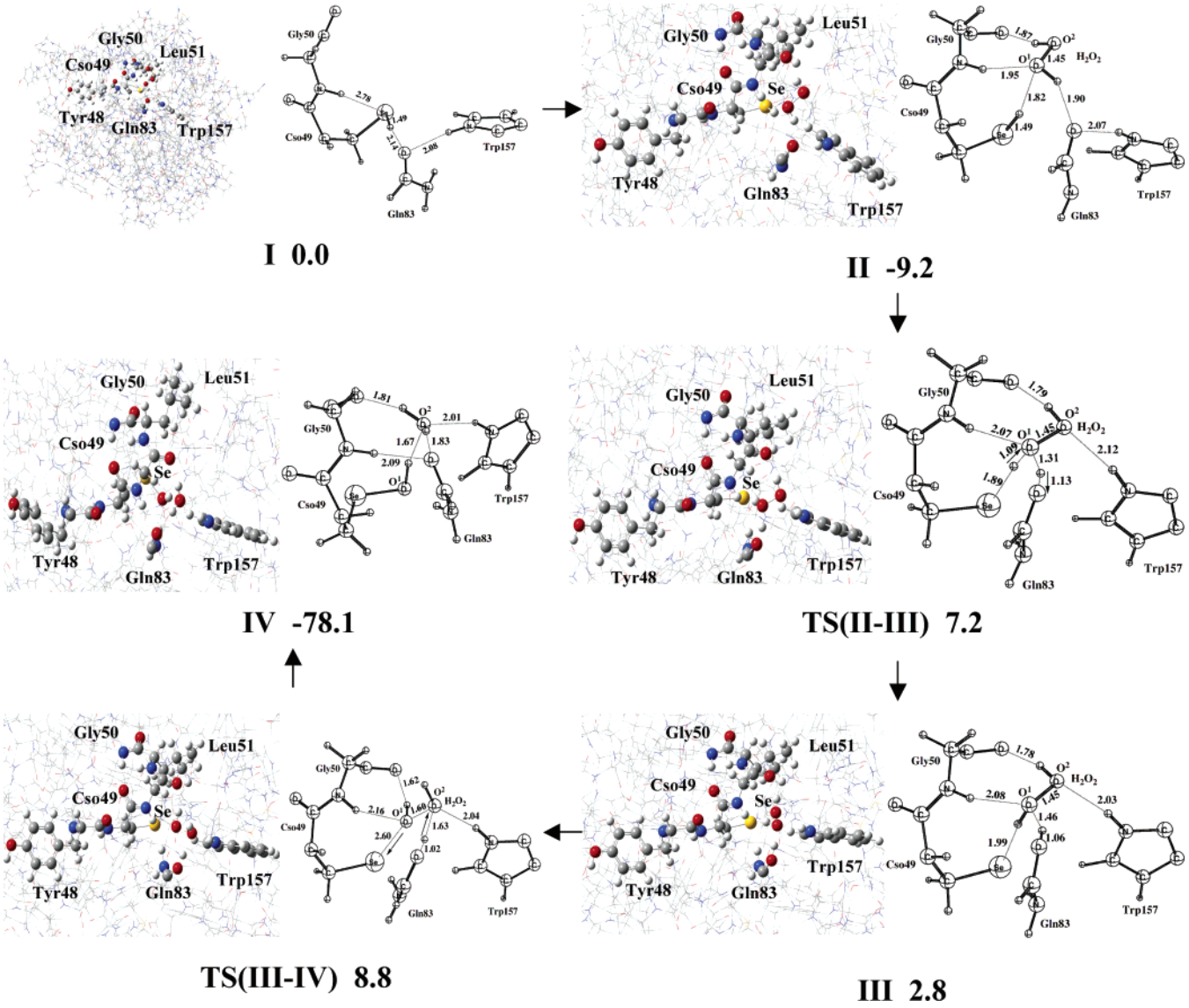

Figure 2. Optimized ONIOM structures (C atoms in gray, H atoms in white, and O and N atoms in black) with critical reaction coordinates (separately displayed in the adjoining views, in Å) and energies (in kcal/mol) of the reactant, intermediates, transition states, and product for the H_2O_2 reduction mechanism of GPx.

III. Results and Discussions

In a recent study, we investigated the catalytic mechanism of hydrogen peroxide reduction using the active site only QM approach.[26] The most relevant results of that study are:

(1) According to experimental data,[21] the active state of the selenocysteine residue could be either the selenolate anion (E−Se$^-$) or selenol (E−SeH). Our calculations showed that the E−SeH is the most preferable active form of the enzyme.[26]

(2) From the X-ray structure,[22] the geometry optimization led to two different conformers of the Gln83 residue in the active site only model (either the oxo or the $-NH_2$ group of Gln83 facing Trp157), while Trp157 deviated significantly from its position in the X-ray structure.

(3) In general, the formation of selenenic acid (E−Se−OH) could occur either via a concerted or a stepwise mechanism. Our calculations using the active site only models show that the barrier for the concerted mechanism is 4.2 kcal/mol higher than that for the stepwise mechanism.[26]

In the present ONIOM (QM:MM) study, the aforementioned theoretical conclusions from the previous study are fully utilized to investigate the reaction mechanism of H_2O_2 reduction catalyzed by GPx; here we only investigate the mechanisms that were identified to be plausible in the active site only study.

A. Hydrogen Peroxide Coordination. The starting point of our studies is the optimization of the structure of the enzyme. The ONIOM calculations show that, in contrast to the active site only study, in the presence of the surrounding protein these calculations yield only a single stable conformation of Gln83, structure **I** (Figure 2). It was found that during the optimization both the Gln83 and the Trp157 residues largely retain their positions from the X-ray structure. The effect of the protein environment on the structure of the active site is also reflected in the RMS deviations between the optimized and the X-ray structures, which are 1.48 and 0.97 Å for the active site only and QM/MM calculations, respectively.

In the first step of this reaction, similarly as for the active site only system, a hydrogen peroxide molecule coordinates to the active site of the enzyme to produce **II** (Figure 2). In **II**, H_2O_2 forms strong hydrogen bonds with the Cso49, Gln83, and Gly50 residues and has a binding energy of 9.2 (6.3) kcal/mol. In the presence of the protein environment the SeH−O^1 bond (1.82 Å) is shorter than the corresponding bond (1.91 Å) in the

active site only system. As discussed above, in the present study we did not include a water molecule in the active site, which in the case of active site only investigations was shown to reduce the H_2O_2 binding energy by 1.0 kcal/mol. The RMS deviation between the MM parts of structures **I** and **II** is only 0.09 Å, which indicates that hydrogen peroxide binds to the active site without affecting the surrounding protein environment.

B. Formation of Selenenic Acid (E−Se−OH). In the next stage of the reaction, the selenenic acid (E−Se−OH) is formed. Since in our previous active site only study, it was shown that the calculated barrier for the concerted mechanism of the selenenic acid E−Se−OH is a 4.2 kcal/mol higher than that for the stepwise mechanism, in the present study we investigate only the latter mechanism at the ONIOM level. As shown previously, the stepwise mechanism consists of the two steps: (a) formation of selenolate anion ($E-Se^-$) and (b) O−O bond cleavage.

1. Formation of the Selenolate Anion (E−Se⁻). In the first step, the formation of the selenolate anion ($E-Se^-$) occurs via the proton transfer from the Se through the oxygen (O^1) atom of hydrogen peroxide to the neighboring Gln83, leading to the intermediate **III** (Figure 2). In this process the Gln83 residue is seen to play the role of proton acceptor. This proposal concerning the participation of the Gln83 residue in the reaction is consistent with the available experimental information.[32] The computed barrier for the creation of the selenolate anion from structure **II** is 16.4 (12.8) kcal/mol. However, this value of the barrier height could be slightly overestimated because B3LYP is known to overestimate the activation energy for long-range proton-transfer processes.[42] The fully optimized transition state structure (**TS(II−III)**) associated with this barrier is shown in Figure 2. As seen from this figure, **TS(II−III)** is stabilized by the hydrogen bonds from the Gly50, Gln83, Trp157, and Cso49 residues. In the presence of the surrounding protein, Trp157 forms a hydrogen bond with H_2O_2, whereas in the active site only study Trp157 is hydrogen-bonded to Gln83. In comparison to the active site only study, the $Gln83H^+-O^1$ and $Se-O^1H$ bond distances are longer by 0.05 and 0.03 Å, respectively. This step is calculated to be endothermic by 12.0 (9.5) kcal/mol. The correction introduced for the different atom types between the structures **II** and **III** (in the present case from HS to HO type) reduce the endothermicity by 1.7 kcal/mol. In intermediate **III**, the O−H bond length in the protonated Gln83 is 1.05 Å, which is 0.03 Å smaller than that in the active site only study. The absence of the active site water molecule slightly increases both barrier and exothermicity by 1.0 and 1.1 kcal/mol, respectively, in the active site only calculations. The RMS deviations between the MM parts of **II**−**TS(II**−**III)** and **II**−**III** structures are 0.20 and 0.21 Å, respectively.

2. O−O Bond Cleavage. In the second step of the stepwise mechanism, the O^1-O^2 bond of H_2O_2 is cleaved. During this process, one hydroxyl fragment (O^1H) is transferred to the selenolate anion ($R-Se^-$) to form selenenic acid ($R-SeO^1H$), while simultaneously the second hydroxyl fragment (O^2H) accepts the previously transferred proton from Gln83 to form a water molecule (**IV**, Figure 2).

The optimized transition state (**TS(III−IV)**) for this process is shown in Figure 2. As seen from this figure, all the corresponding distances indicate that this process is synchronous. The calculated barrier for this process is 6.0 (7.6) kcal/mol. In comparison to the active site only study, the $Se-O^1$ and $Trp157-O^2$ bond distances are shorter by 0.11 and 0.43 Å, respectively. Since this step follows the 12.0 kcal/mol endothermic selenolate anion formation step (from **II** to **III**), the overall barrier (from **II** to **IV**) for the formation of selenenic acid (E−Se−OH) becomes 18.0 (17.3) kcal/mol. These results show that the presence of surrounding protein slightly increases the overall barrier by 0.7 kcal/mol, which is still in a good agreement with the experimentally measured barrier of 14.9 kcal/mol.[25] Here, it has to be stressed that the active site is not deeply buried inside the enzyme; instead it is located on the interface of two monomers, which is the main reason the inclusion of protein surroundings does not exert any significant influence on the energetics of the reaction. However, in methane monooxygenase, cytochrome P450, and triosephosphate isomerase enzymes, where active sites are deeply buried, the protein surroundings has been reported to exhibit considerable effects.[14] The absence of the water molecule at the active site increases the barrier by 2.0 kcal/mol. This step of the stepwise formation of selenenic acid is calculated to be exothermic by 80.9 (66.6) kcal/mol. Here, the effect from changing MM atom types (from O2 to OS) is 1.4 kcal/mol. The RMS deviations between the MM parts of the **III**−**TS(III**−**IV)** and **III**−**IV** structures are 0.15 and 0.28 Å, respectively, again indicating that there are no major changes in the protein environment in this step of the mechanism.

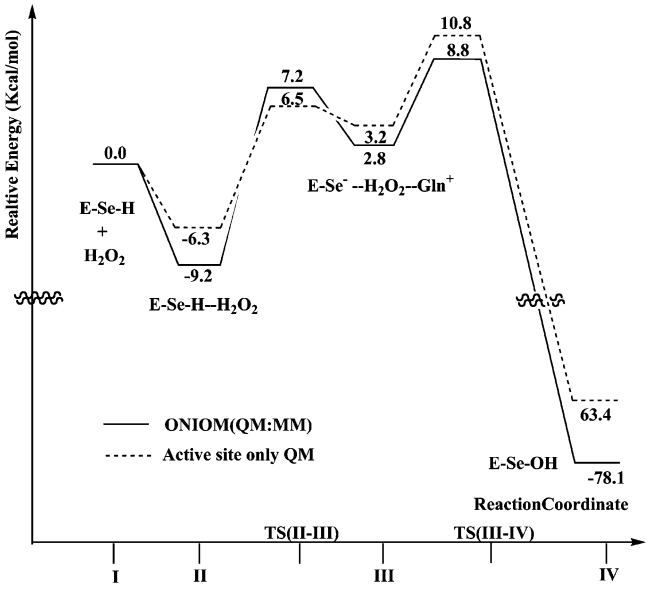

Figure 3. Potential energy diagram for the H_2O_2 reduction mechanism of GPx (including solvent effects). In this diagram, the active site only energies are taken from ref 26.

IV. Summary and Conclusions

In the present study, to treat critical protein−active site interactions, the reaction mechanism of hydrogen peroxide reduction catalyzed by GPx has been studied using the entire monomer as a model. A newly developed optimization scheme that allows full optimization of transition states for large systems has been utilized. The entire GPx monomer contains 3113 atoms in 196 amino acid residues. The energy diagram for the H_2O_2 reduction by GPx is shown in Figure 3.

In the first part of this reaction, H_2O_2 coordinates to the active site of the enzyme (**I**) to produce **II**. This step is found to be exothermic by 9.2 (6.3) kcal/mol. In this step, in a marked contrast to the active site only models, the presence of the surrounding protein in the ONIOM(QM:MM) calculations provides only a single stable conformation of Gln83. Furthermore, in the latter case we find much better resemblance between the optimized and X-ray structure.

The second part of the selenenic acid (E−Se−OH) formation is divided into the following two steps: (a) formation of selenolate anion (E−Se^-) and (b) O−O bond cleavage. In the first step, the Se−H bond of the selenol (R−Se^-) is cleaved and simultaneously the proton is transferred through the oxygen (O^1) atom of hydrogen peroxide to Gln83 to generate **III**. The role of Gln83 is in line with the experimental proposal that this residue participates in the catalytic cycle.[32] This step has a barrier of 16.4 (12.8) kcal/mol corresponding to **TS(II−III)** and is endothermic by 12.0 (9.5) kcal/mol. In the second step, the O^1-O^2 bond of H_2O_2 is broken, and a hydroxyl group (O^1H) is transferred to the selenolate anion (R−Se^-) to form selenenic acid (R−SeO^1H) and a water molecule (**IV**). The calculated barrier for this process, see **TS(III−IV)**, is 6.0 (7.6) kcal/mol, and it is exothermic by 80.9 (66.6) kcal/mol. The overall barrier (from **II** to **IV**) for the formation of E−Se−OH is 18.0 (17.3) kcal/mol and is in a reasonable agreement with the experimentally measured barrier of 14.9 kcal/mol.[25] Since in GPx the active site is located at the enzyme surface away from the surrounding protein, the effect of the protein environment on the barrier is only 0.70 kcal/mol. However, in enzymes such as methane monooxygenase, cytochrome P450, and triosephosphate isomerase, where active sites are deeply buried, the protein surroundings has been calculated to cause significant reduction in barriers.[14]

Moreover, the present study is the first example to exhibit the applicability of the newly developed coupled macro/microiteration optimization method in the investigation of enzymatic reactions using the ONIOM method for a realistic enzyme model. The present study will pave the path for more QM/MM studies to elucidate enzymatic mechanisms.

Acknowledgment. This work was supported in part by a grant (CHE-0209660) from the National Science Foundation. A DURIP grant (FA9550-04-1-0321) from the AFOSR is also acknowledged for support of the computer facilities. The use of computational resources at the Cherry Emerson Center for Scientific Computation is also acknowledged.

References and Notes

(1) Prabhakar, R.; Morokuma, K.; Musaev, D. G. *J. Comput. Chem.* **2005**, *26*, 443−446.
(2) Siegbahn, P. E. M.; Blomberg, M. R. A. *Chem. Rev.* **2004**, *100*, 421−437.
(3) de Visser, S. P.; Kumar, D.; Cohen, S.; Shacham, R.; Shaik, S. *J. Am. Chem. Soc.* **2004**, *126*, 8362−8363.
(4) Noodleman, L.; Lovell, L. T.; Han, W.; Li, J.; Himo, F. *Chem. Rev.* **2004**, *104*, 459−508.
(5) Basch, H.; Mogi, K.; Musaev, D. G.; Morokuma, K. *J. Am. Chem. Soc.* **1999**, *121*, 7249−7256.
(6) Musaev, D. G.; Basch, H.; Morokuma, K. *J. Am. Chem. Soc.* **2002**, *124*, 4135−4148.
(7) Prabhakar, R.; Siegbahn, P. E. M. *J. Am. Chem. Soc.* **2004**, *107*, 3944−3953.
(8) Baik, M.-H.; Newcomb, M.; Friesner, R. A.; Lippard, S. J. *Chem. Rev.* **2003**, *103*, 2385−2420.
(9) Shaik, S.; Kumar, D.; de Visser, S. P.; Altun, A.; Thiel, W. *Chem. Rev.* **2005**, *105*, 2279−2328.
(10) (a) Gao, J. *Rev. Comput. Chem.* **1996**, *7*, 119−185. (b) Warshel, A.; Karplus, M. *J. Am. Chem. Soc.* **1972**, *94*, 5612. (c) Warshel, A. *Computer Modeling of Chemical Reactions in Enzymes and Solutions*; Wiley: New York, 1991.
(11) Schoeneboom, J. C.; Cohen, S.; Lin, H.; Shaik, S.; Thiel, W. *J. Am. Chem. Soc.* **2004**, *126*, 4017−4034.
(12) Guallar, V.; Friesner, R. A. *J. Am. Chem. Soc.* **2004**, *126*, 8501−8508.
(13) Shurki, A.; Warshel, A. *Adv. Protein Chem.* **2003**, *66*, 249−313.
(14) Friesner, R. A.; Gullar, V. *Annu. Rev. Phys. Chem.* **2005**, *56*, 389−427.
(15) Maseras, F.; Morokuma, K. *J. Comput. Chem.* **1995**, *16*, 1170−1179.
(16) Dapprich, S.; Komaromi, I.; Byun, S.; Morokuma, K.; Frisch, M. J. *J. Mol. Struct. (THEOCHEM)* **1999**, *461*, 1−23.
(17) Bakowies, D.; Thiel, W. *J. Phys. Chem.* **1996**, *100*, 10580.
(18) Klähn, M.; Braun-Sand, S.; Rosta, E.; Warshel, A. *J. Phys. Chem. B* **2005**, *109*, 15645−15650.
(19) Mills, G. C. *J. Biol. Chem.* **1957**, *229*, 189−197.
(20) Flohè, L. In *Glutathione*; Dolphin, D., Avramovic, O., Poulson, R., Eds.; John Wiley & Sons: New York, 1989; pp 644−731.
(21) Epp, O.; Ladenstein, R.; Wendel, A. *Eur. J. Biochem.* **1983**, *133*, 51−69.
(22) Ren, B.; Huang, W.; Åkesson, B.; Ladenstein, R. *J. Mol. Biol.* **1997**, *268*, 869−885.
(23) Prabhakar, R.; Musaev, D. G.; Khavrutskii, I. V.; Morokuma, K. *J. Phys. Chem. B* **2004**, *108*, 12643−12645.
(24) Flohé, L.; Loschen, G.; Gunzler, W. A.; Eichele, E. *Hoppe−Seylers's Z. Physiol. Chem.* **1972**, *353*, 987−999.
(25) Roy, G.; Nethaji, M.; Mugesh, G. *J. Am. Chem. Soc.* **2004**, *126*, 2712−2713.
(26) Prabhakar, R.; Vreven, T.; Morokuma, K.; Musaev, D. G. *Biochemistry* **2005**, *44*, 11864−11871.
(27) Vreven, T.; Frisch, M. J.; Kudin, K. N.; Schlegel, H. B.; Morokuma, K. *Mol. Phys.* **2006**, *104*, 701−714.
(28) Vreven, T.; Frisch, M. J., to be submitted for publication.
(29) Baker, J. *J. Comput. Chem.* **1986**, *7*, 385.
(30) Vreven, T.; Morokuma, K.; Farkas, Ö.; Schlegel, H. B.; Frisch, M. J. *J. Comput. Chem.* **2003**, *24*, 760−769.
(31) *GaussianView*, version 3.0; Gaussian, Inc.; Pittsburgh, PA, 2003.
(32) Ursini, F.; Maiorino, M.; Brigelius-Flohé, R.; Aumann, K. D.; Roveri, A.; Schomburg, D.; Flohé, L. *Methods Enzymol.* **1995**, *252*, 38−53.
(33) Frisch, M. J.; Trucks, G. W.; Schlegel, H. B.; Scuseria, G. E.; Robb, M. A.; Cheeseman, J. R.; Montgomery, J. A., Jr.; Vreven, T.; Kudin, K. N.; Burant, J. C.; Millam, J. M.; Iyengar, S. S.; Tomasi, J.; Barone, V.; Mennucci, B.; Cossi, M.; Scalmani, G.; Rega, N.; Petersson, G. A.; Nakatsuji, H.; Hada, M.; Ehara, M.; Toyota, K.; Fukuda, R.; Hasegawa, J.; Ishida, M.; Nakajima, T.; Honda, Y.; Kitao, O.; Nakai, H.; Klene, M.; Li, X.; Knox, J. E.; Hratchian, H. P.; Cross, J. B.; Bakken, V.; Adamo, C.; Jaramillo, J.; Gomperts, R.; Stratmann, R. E.; Yazyev, O.; Austin, A. J.; Cammi, R.; Pomelli, C.; Ochterski, J. W.; Ayala, P. Y.; Morokuma, K.; Voth, G. A.; Salvador, P.; Dannenberg, J. J.; Zakrzewski, V. G.; Dapprich, S.; Daniels, A. D.; Strain, M. C.; Farkas, O.; Malick, D. K.; Rabuck, A. D.; Raghavachari, K.; Foresman, J. B.; Ortiz, J. V.; Cui, Q.; Baboul, A. G.; Clifford, S.; Cioslowski, J.; Stefanov, B. B.; Liu, G.; Liashenko, A.; Piskorz, P.; Komaromi, I.; Martin, R. L.; Fox, D. J.; Keith, T.; Al-Laham, M. A.; Peng, C. Y.; Nanayakkara, A.; Challacombe, M.; Gill, P. M. W.; Johnson, B.; Chen, W.; Wong, M. W.; Gonzalez, C.; Pople, J. A. *Gaussian 03*; Gaussian, Inc.: Wallingford, CT, 2004.
(34) (a) Becke, A. D. *Phys. Rev. A* **1988**, *38*, 3098−3100. (b) Lee, C.; Yang, W.; Parr, R. G. *Phys. Rev. B* **1988**, *37*, 785−789. (c) Becke, A. D. *J. Chem. Phys.* **1993**, *98*, 5648−5652.
(35) The partial charges and bonding parameters required to describe the selenocysteine residue have been obtained from B3LYP/6-31G(d) calculations on 2-acetylamino-2-methylcarbamoylethaneseleninic acid, using standard Amber RESP and force constant estimation procedures.
(36) Vreven, T.; Byun, K. S.; Komáromi, I.; Dapprich, S.; Montgomery, J. A., Jr.; Morokuma, K.; Frisch, M. J. *J. Chem. Theory Comput.* **2006**, *2*, 815−826.
(37) Vreven, T.; Morokuma, K. *Annu. Rep. Comput. Chem.*, in press.
(38) Vreven, T.; Morokuma, K. *Theor. Chem. Acc.* **2003**, *109*, 125−132.
(39) Torrent, M.; Vreven, T.; Musaev, D. G.; Morokuma, K.; Farkas, Ö.; Schlegel, H. B. *J. Am. Chem. Soc.* **2002**, *124*, 192−193.
(40) Kwiecien, R. A.; Khavrutskii, I. V.; Musaev, D. G.; Morokuma, K.; Banerjee, R.; Paneth, P. *J. Am. Chem. Soc.* **2006**, *128*, 1287−1292.
(41) Li, J.; Cross, J. B.; Vreven, T.; Meroueh, S. O.; Mobashery, S.; Schlegel, H. B. *Proteins* **2005**, *61*, 246−257.
(42) Prabhakar, R.; Blomberg, M. R. A.; Siegbahn, P. E. M. *Theor. Chem. Acc.* **2000**, *104*, 461−470.